Paper 4701-36, Proceedings of the SPIE Smart Structures and Materials Symposium, San Diego, CA, March 18-21, 2002

Analysis and Simulation of the Ultrasonic/Sonic Driller/Corer(USDC)

Xiaoqi Bao, Zensheu Chang, Stewart Sherrit, Benjamin P. Dolgin, Yoseph Bar-Cohen, (JPL/Caltech, Pasadena, CA 91109)
Dharmendra S. Pal, Shu Du, Thomas Peterson (Cybersonics, Erie, Pa 16510)

ABSTRACT

An ultrasonic/sonic driller/corer (USDC) was developed to address the challenges to the NASA objective of planetary in-situ rock sampling and analysis. The USDC uses a novel drive mechanism, transferring ultrasonic vibration into impacts on a drill stem at sonic frequency using a free-flying mass block (free-mass). The main parts of the device and the interactions between them were analyzed and numerically modeled to understand the drive mechanism and allow design of effective drilling mechanism. A computer program was developed to simulate the operation of the USDC and successfully predicted the characteristic behavior of the new device. This paper covers the theory, the analytical models and the algorithms that were developed and the predicted results.

Keywords: Piezoelectric Ultrasonic Drill, Piezoelectric Actuators, Rock Sampling, FE Analysis, Numerical Simulation.

1. INTRODUCTION

Rock drilling and sampling are required by NASA exploration missions to Mars, Titan, comets and asteroids for in-situ analysis. Existing drilling techniques are limited by the needs for large axial forces and holding torques, high power consumption and an inability to efficiently duty cycle. Lightweight robots and rovers have difficulties accommodating these requirements. To address these key challenges to the NASA objective of planetary in-situ rock sampling and analysis, an ultrasonic/sonic driller/corer (USDC) was developed [1,2]. The actuator of the USDC is an ultrasonic horn transducer that is driven by a piezoelectric stack. Unlike the typical ultrasonic drill where the drill stem is acoustically coupled to the transducer, the horn transducer in the USDC drives a free flying mass (free-mass), which bounces between the horn tip and a drill stem at sonic frequencies. The impacts of the free-mass create stress pulses that propagate to the interface of the stem tip and the rock. The rock fractures when its ultimate strain is exceeded at the rock/bit interface. This novel drilling mechanism has been shown to be more efficient and versatile than conventional ultrasonic drills under a variety of conditions. The low mass of a USDC device and the ability to operate with minimum axial load with near zero holding torque (see Fig. 1) offers an important tool for sample acquisition and in-situ analysis.

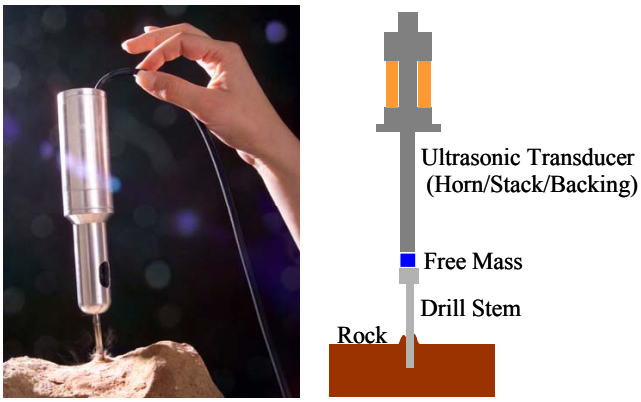

Fig. 1. The USDC is shown coring with minimum axial force and holding torque (left), and a schematic diagram of the USDC device (right).

In order to understand the drive mechanism and allow design of effective drilling mechanism, a computer model was developed. Hear are five elements involved in the drilling i.e. the electrical driver, ultrasonic transducer, free-mass, drill stem, and the rock. In the initial modeling the main elements and the interaction between them were analyzed and modeled separately. An integrated one-dimensional software program was developed to simulate the operation of the USDC. The strain that is induced in the rock was calculated and the drilling rate was estimated based on the specific energy required to fracture the rock. This paper reports on the individual models and the algorithms of the integrated program. The computed results and the comparison with the experimental tests are also presented.

2. NUMERICAL MODELING AND ANALYSIS

The USDC device consists of three main parts: an ultrasonic transducer (piezoelectric stack, a backing element, and a horn), free-mass and a drill stem. The ultrasonic transducer vibrates at a frequency of about 20kHz. These vibrations of the horn tip excite the free-mass, causing it to hop between the horn tip and the top of the drill stem at frequencies around 1000-Hz. The free-mass transfers energy from the ultrasonic transducer to the drill stem. The shock waves caused by the impacts of the free-mass propagate to the bit/rock interface and wherever the rock is strained past its ultimate strain it fractures. In order to determine the critical issues related to the control and optimization of the drill models the interaction at the various interfaces of the drill were investigated. The four interactions that were modeled include: 1) transducer with the driving circuit, 2) horn tip with the free-mass, 3) free-mass with the drill stem and 4) base of the drill stem (bit) with the rock. In order to integrate these models into a computer program to simulate the operation of the USDC, efforts were made to simplify the models and reduce the computing time.

A. Modal analysis and equivalent circuit of the transducer

The horn transducer consists of a steel-backing block, a PZT-8 stack, a steel horn and a pre-stress bolt as shown in Fig. 2.

The transducer is a composite longitudinal vibrator with varying cross sections and can be modeled by the Mason equivalent circuit as presented in a previous paper [3]. In order to include engineering details in the final transducer design a finite element model was developed to determine the full frequency response of the device.

The finite element equations for elastic structure including piezoelectric elements have been derived by many authors [4,5]. In this high power ultrasonic application, the transducer is designed and fabricated to have high mechanical Q, and is operated at or near its first longitudinal resonance frequency. Using modal analysis allowed us to isolate and concentrate on this resonance mode and it simplifies the model and reduces the computing time.

Solving the generalized eigenvalue problem of finite element equations, the resonance frequencies and corresponding mode shapes can be found. We obtain a set of resonance frequencies, $\omega_1, \omega_2, \ldots, \omega_n$ and normalized mode shapes (eigenvictors)

$$\{\xi_1\}, \{\xi_2\}, \ldots, \{\xi_n\}.$$

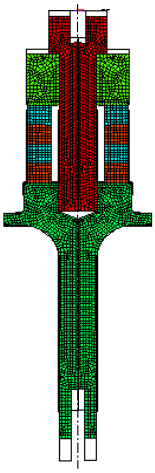

Fig. 2. Calculated modal shape of the horn transducer at frequency of 22.668 kHz. The meshed areas represent the cross section of the deformed transducer

Finite element packages that can be used to determine these resonance frequencies and mode shapes are available commercially. The horn transducer of the USDC was modeled by axisymmetric elements in Ansys finite element package [7]. Fig. 2 shows the model shape of the first nonzero-frequency resonance of the transducer obtained by the finite element model. The mode is basically a longitudinal vibration displacement at the horn tip than the back. The frequency is 22.688 kHz, which is very close to the frequencies from 22 to 23 kHz.

By expressing the displacement as the summation of shapes as

$$\{\xi\} = \sum_n d_i \{\xi_i\}$$

the finite equations can be converted to a modal equations as was done in previous work [6]

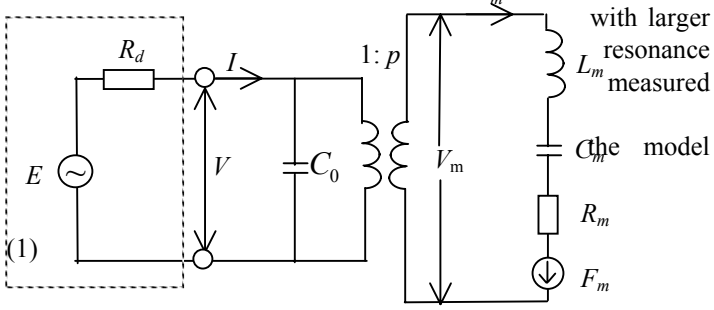

Fig. 3. Schematic of the equivalent circuit of the transducer around resonance. The generator source is also included in the dashed square.

$$(\omega_i^2 + j\omega R_i - \omega^2)d_i = p_i V + Fm_i$$
$$Q = \sum_n p_i d_i + C_0 V \qquad i = 1, \ldots, n \quad (2)$$

where d_i is the amplitude of the mode i, Q is the electric charge on the electrode, R_i, p_i and Fm_i are effective damping, electromechanical coupling and force for the modes respectively. The R_i and p_i can be calculated from the matrixes [C] and [P], and Fm_i is expressed as

$$Fm_i = \{\xi_i\}^T \{F\} \quad (3)$$

Only the first longitudinal mode is taken into account in the analysis. Then, Eq.(2) becomes

$$(\omega_1^2 + j\omega R - \omega^2)d = pV + Fm$$
$$Q = pd + C_0 V \quad (4)$$

where subscripts of 1 are omitted for simplification except that for resonance frequency ω_1.

The Eqs. (4) is able to be represented by an equivalent circuit around resonance as is shown in Fig. 3.

In Fig. 3, subscripts *m* are added to denote that the symbols actually represent mechanical variables and parameters. The element in the dashed square is the sketch of electric driving circuit.

Upon inspection we have $L_m = 1$, $C_m = 1/\omega_1^2$ and the mechanical "current" I_m is the modal velocity

$$I_m = \dot{d} \,. \quad (5)$$

This circuit allows us to calculate the variables easily. When the transducer is driven electrically and is mechanically unconstrained (no impacts with the free-mass), the modal velocity can shown to be

$$I_m = \frac{pV}{j(\omega L_m - \frac{1}{\omega C_m}) + R_m} \quad (6)$$

B. Reaction of free-mass impacts to the transducer

In the operation of the USDC, a small preload force, either from gravity or from a spring is applied to the transducer. The force pushes the transducer down toward the free-mass and the bit. A harmonic voltage at a frequency around the resonance drives the transducer. The free-mass, energized by the vibrating horn tip, then, bounces between the bit and horn tip and maintains a gap between them. The impacts of the free-mass to the horn tip effect both vibration and translation movements of the horn transducer.

1) Translation movement of the horn transducer

We assume the preload force is constant and produces an acceleration a of the transducer. Suppose an impact happens at time t_I, and contact time is very short, the contact force can be expressed as

$$F_c = f_I \delta(t - t_I) \quad (7)$$

where δ is the delta function. Using momentum conservation in the impact, we have

$$f_I = -m\Delta v_I \quad (8)$$

where m and Δv_I is the mass and velocity of the free-mass respectively. Each impact results in a change of the center of mass (COM) velocity of the horn by

$$\Delta U_I = \frac{-m\Delta v_I}{M} H(t - t_I) \qquad (9)$$

where M is the total mass of the horn transducer, and H is the step function. Therefore, the COM velocity of the transducer becomes

$$U = U_0 + at + \sum_I \Delta U_I \qquad (10)$$

The displacement of the transducer is therefore the time integral of the velocity.

2) Vibration of the transducer

The vibration of the transducer is the summation of the vibration induced by the electric voltage *V* and the vibration caused by the mechanical force F_m, which are the impact forces of the free-mass. The applied voltage is assumed being harmonic in the form of $V = V_0 \exp(j\omega t)$. The induced vibration can be solved explicitly upon the circuit. To calculate the impact induced vibration, we rewrite the equation of the equivalent circuit in the form of differential equation as

$$L_m \ddot{d} + R_m \dot{d} + C_m d = pV(t) + F_m \qquad (11)$$

The mechanical force caused by the impacts of the free-mass on the horn tip can be determined from Eq. (3), Eq. (7) and (8), to be

$$F_m = \xi_t f \delta(t - t_I) = -m\Delta v_I \xi_t \delta(t - t_I) \qquad (12)$$

where ξ_t is the tip displacement of the mode shape. The solution of Eq.(11) for the impact force F_m is a free ring-down vibration after the impact time t_I and is expressed as

$$I_{mI} = \dot{d}_I = -\frac{m\Delta v_I \xi_t}{L_m} \exp[(-\alpha + j\omega_f)(t - t_I)], \quad t > t_I \qquad (13)$$

where α is damping coefficient and ω_f is the free vibration frequency, and can be determined by the circuit with the electric source $E = 0$.
The final solution of the model velocity is

$$I_m = \dot{d} = \dot{d}_e + \sum_I \dot{d}_I = I_{me} + \sum_I I_{mI} \qquad (14)$$

where the subscript *e* is denote to the electrically induced variables and *I* to the impact induced.

C. Interaction between transducer and the electric driver

Power output from the voltage source E is the time averaged integral of product of multiplication of the source voltage by the current and is expressed as

$$P_E = \frac{1}{T}\int_T E(t)I(t)dt$$
$$= \frac{1}{T}\int_T E(t)I_e(t)dt + \frac{1}{T}\int_T E(t)\sum_I I_I(t)dt \quad (15)$$

or

$$P_E = P_{Ee} + P_{EI} \quad (16)$$

where the first item in Eq.(16), P_{Ee}, is the power with no free-mass loading and P_{EI} is the power change introduced by the free-mass loading. $I_e(t)$ is the current though the source due to the electric drive voltage, and $I_I(t)$ is the current due to the free-mass impacts,

The power lost on the resistor R_d is calculated by

$$P_d = \frac{1}{T}\int_T R_d[I(t)]^2 dt = \frac{R_d}{T}\int_T [I_e(t) + \sum_I I_I(t)]^2 dt \quad (17)$$

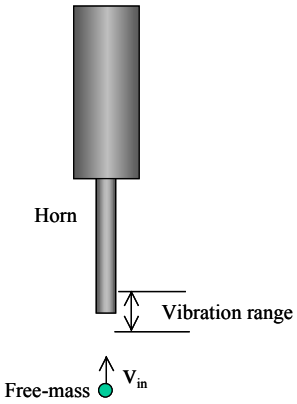

Fig. 4. A Schematic of the horn driving the free-mass.

D. Free-mass driven by the horn transducer

1) Simple collision model

A simple collision model was applied first to explore the basic mechanism of the horn/free-mass driving. In this model, we assume that the energy loss and time duration of the impact is negligible, and the mass of the horn is much larger than the free-mass. Using the conservation of momentum and energy, we have

$$v_{out} = v_{in} + 2v \quad (18)$$

where v_{in} is the incoming velocity of free-mass prior to impact with the horn, v_{out} is the outgoing velocity after impact with the horn, and v is the velocity of the horn tip.

The horn vibrates at the resonance frequency. The tip displacement is harmonic and is represented by

$$u = u_0 \cos(\omega t + \vartheta) \quad (19)$$

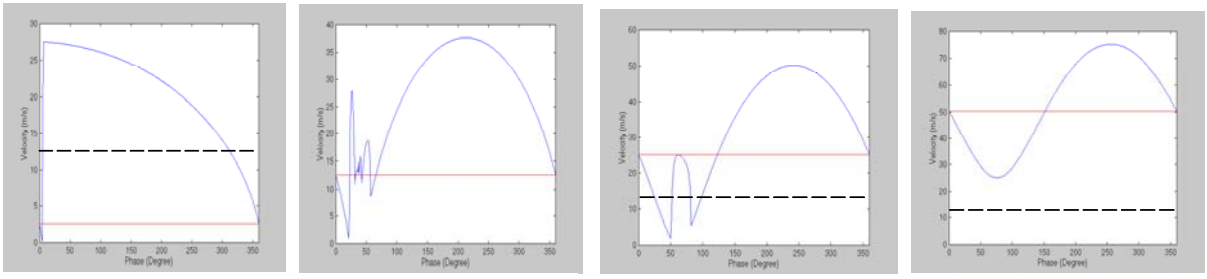

a. $v_{in} = 0.2\ v_t$ b. $v_{in} = 1.0\ v_t$ c. $v_{in} = 2.0\ v_t$ d. $v_{in} = 4.0\ v_t$

Fig. 5. The speed of the free-mass after impact versus relative tip vibration phase for different incoming speeds. The solid horizontal lines indicate the level of free-mass incoming speed, and the dashed line is the amplitude of tip velocity v_t.

where time zero is set at the moment when the free-mass just reaches the edge of the range of tip vibration. The velocity of the horn tip is found by taking the time derivative of the displacement and can be written as

$$v = -\omega u_0 \sin(\omega t + \vartheta) \qquad (20)$$

A computer simulation model, which traces the position of the free-mass until it leaves the tip vibration range ($2u_0$), was programmed. The routine calculates the free-mass speed after interaction with the horn. The outgoing speeds of the free-mass versus the vibration phase are shown in the Fig. 5 for different ratios of incoming speed to the tip velocity amplitude respectively. The model accounts for multiple impacts that become possible when the impact is timed appropriately, which are sown in Fig. 6b and 6c at phases around 50°.

Although the Eq.(18) implies that the v_{out} may be less than v_{in} when the tip velocity v is negative, the computed results show that the free-mass velocity does increase on average after interaction with the vibrating tip assuming a uniform probability of the relative phase in the range of 0° – 360°. The increase rate is higher the lower the relative incoming speed. The causes of the increase are

(1) Although the tip velocity alternates periodically and is negative half of the time, the free-mass has less chance to interact with the tip when the tip is pulling back, especially if the free-mass speed is low. It results the phase range where the $v_{out} > v_{in}$ is always greater than the half of 360°.

(2) If the first impact results in low or negative v_{out}, the free-mass will stay in the tip vibration range longer and has the possibility to be hit a second time. The irregularities of the curves around a phase of 50° in Fig. 5b and 5c are due to the multiple impacts between the free-mass and the tip.

2) Finite element model

In the simple collision model, we assumed that the horn mass is much greater than the free-mass. This is true if we include the total mass of the horn transducer. However, in the short time duration that the impact lasts, the impact wave propagates to a limited range within the horn transducer. The remaining part of the transducer is actually not involved in the impact. So, the assumption of a horn mass much greater than the free-mass may not be correct. To explore the details of the real impact/driving process, a finite element model was constructed.

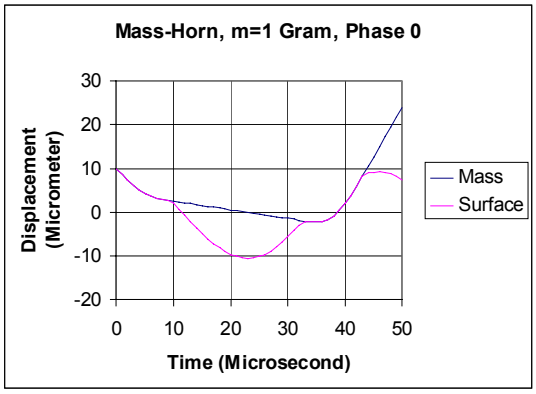

Fig. 7. The free-mass and surface displacement as a function of the time. This figure shows doule contacts happened in the interaction.

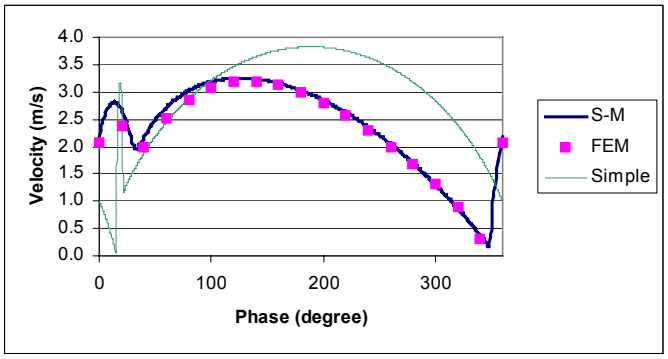

Fig. 8. The velocity of the free-mass as a function of the phase for the simple collision, spring-mass and FEM models.

In the model, the horn transducer is truncated to a λ/4 long bar. A symmetric boundary condition is applied at the other end of the bar. The validity of this truncation is based on the fact that the structure difference in the area far from the point of impact will not make a difference to the free-mass bouncing process. From the view of wave propagation the free-mass should not "feel" the structure difference in the area, as long as the free-mass leaves the tip surface before the impact wave can propagate through the medium and be reflected back to the impact spot. Axisymmetrical solid elements are used to represent the horn tip. The initial conditions, i.e. the displacements and velocities of the nodes, are set to typical longitudinal

vibration values in the bar. Compression only link elements are placed between the nodes on the surfaces of the free-mass and the horn tip in the contact area. The free-mass is treated as a rigid block with a curvature in the contact area.

The finite element approach provides a more accurate description of the free-mass speed after the collision and the time duration of the collision (see Fig. 7). Comparing with the simple collision model (see Fig. 8), ones can see that the maximum speed is typically lower compared to the simple collision model. This implies a limited effective mass of the horn. The curve also displays a phase shift that can be explained by the affect of the contact time.

Spring-mass model

The finite element approach explored two phenomena that were not accounted for in simple collision model, elasticity of the horn and the effective mass involved in the impacts. Based on the phenomena, a spring-mass model was developed. The model uses a mass and two springs to present the horn as shown in Fig. 9.

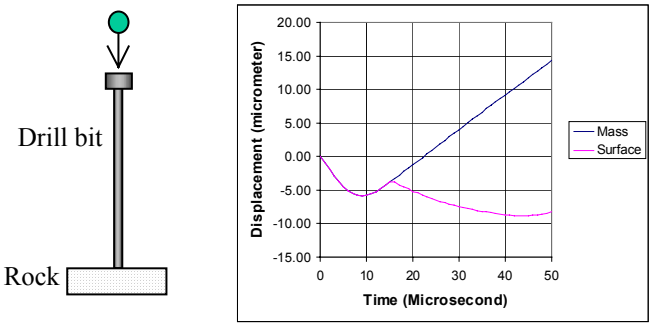

Fig. 10. Finite element displacement results of the free-mass bounce from the drill bit. The free-mass is 2 grams and the incoming speed is 1 m/s. The rebound speed is 0.5 m/s and contact time 15 μs.

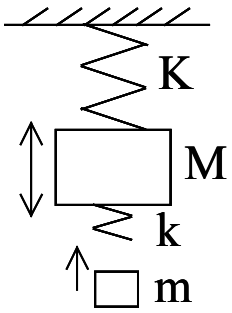

Fig. 9. A sketch of the spring-mass model for horn/free-mass interaction

The parameters of the mass M and front spring k are determined using the rebound velocity and contact time obtained by the finite element approach. The top spring constant K is set by the resonance frequency of the horn transducer. An example of the results of the model is

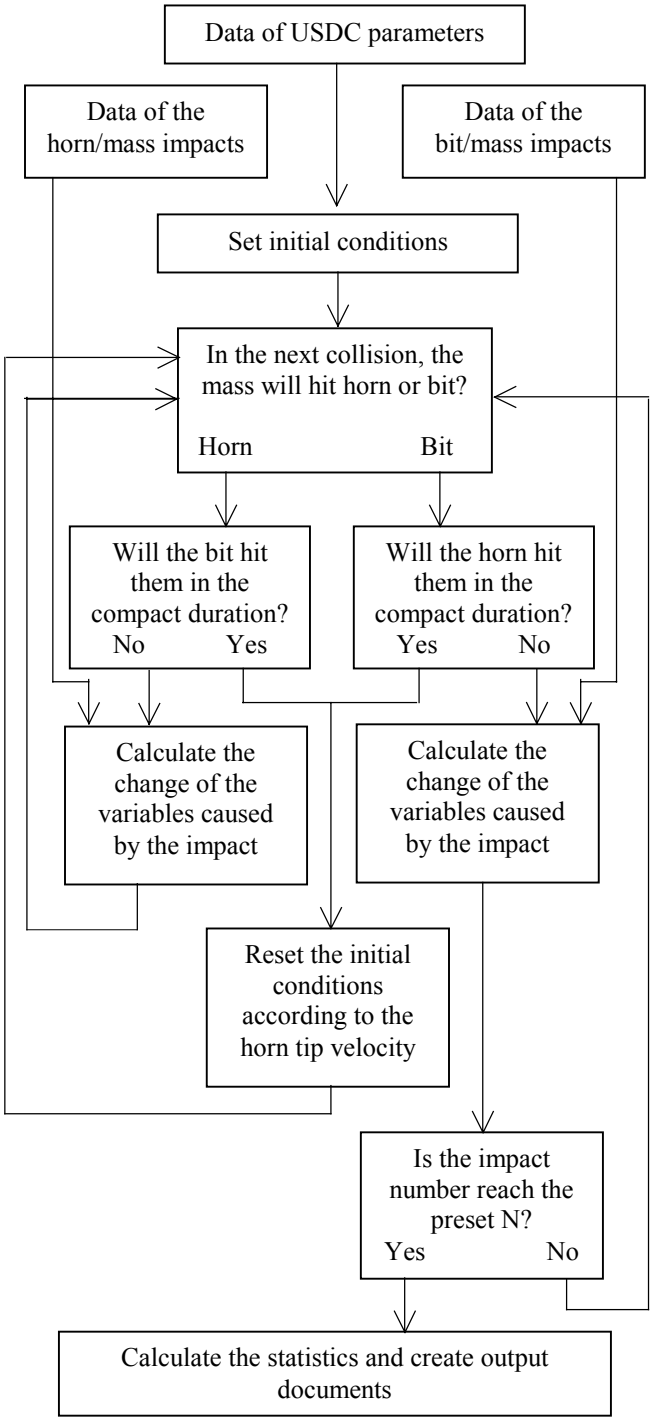

Fig. 12. Flow chart of the simulation program

presented in Fig. 8. The results are found to agree exceptionally well with the finite element results. The spring-mass model therefore provides a more time efficient solution with reasonable accuracy, which was required by the integrated simulation program.

E. Free-mass bouncing from the drill bit

The typical geometry of the drill stem is shown in the left of Fig. 10. It consists of a head and a thin cylindrical bar. The free-mass impacts the head and creates a stress wave that propagates toward the lower end of the bit. A finite element model, which is similar to that used for horn tip and free-mass interaction, was utilized to investigate the impacts. The length of the drill stem was fixed to be long enough to avoid the interference from the reflected wave of the bottom. An example of the results for the displacement of the free-mass and the center of the top surface of drill bit as a function of time is shown in the right of Fig. 10.

The free-mass is 2 grams with speed of 1 m/s. The curvature of free-mass surface at the contact area is 0.1 mm. The steel stem is 3 mm in diameter and has a head of diameter 12 mm and is 6 mm long. The total height of the drill bit is 100 mm. A symmetric boundary condition is applied at the bottom. The rebound speed is 0.5 m/s. The ratio of rebound speed to the incoming speed is dependent on the value of the mass. The affect of the incoming speed is not significant.

By investigating the stress in the stem, we found that the impact resulted in a compression plane wave propagating with a velocity around 5000 m/s, which is in agreement with the longitudinal wave velocity in thin steel bar. The stress at the bottom of the stem is presented in Fig. 11 as a function of time.

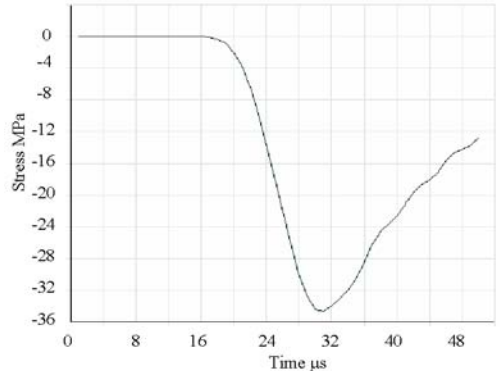

Fig. 11. The stress as a function of time at the bottom of the stem that is 100 mm from the top surface.

F. Integrated computer simulation model

A computer program was developed to simulate the operation of the drill system including the horn transducer, free-mass, drill stem and the electric driver. The program was able to predict the performance of the USDC under a variety of initial conditions.

In the simulation, we assumed that the vibrations in the drill bit induced by the previous free-mass impacts were attenuated when the free-mass returns and hits the drill stem. Initial experiments suggest that this is a valid assumption. We also neglected the movement of the drill stem with respect to the rock, since it is very slow in comparison to the quick motion of the free-mass. Therefore the top surface of the drill stem is set at the same position for the each of the impacts.

The flowchart of the calculation procedure is presented in Fig. 12. We start the simulation by setting the initial values of the position and velocity of the horn and the free-mass. The software traces the translation movements of the horn transducer and the free-mass as well as the vibration of the horn as functions of time. It predicts the time and location of the free-mass/horn or free-mass/bit collision. Using the data of the free-mass/horn and free-mass/bit impacts that were determined from the models mentioned in previous paragraphs, the simulation calculates the changes of the variables as time evolves. The movements and vibration due to the impact are recorded along with the impact momentum and time. The program then proceeds to determine the next impact. The energy supplied by the electric source and delivered to the transducer is integrated and recorded concurrently. The statistics reported by the program include; electric input power, mechanical output power delivered to the drill stem, average and distribution of the free-mass speed, etc. The first 20% of the events are excluded in order to eliminate the possible influence of the initial settings.

Typical simulation results are shown in Fig. 13-15. In this simulation, the transducer is excited by 100 V peak voltage at resonance frequency of 22.5 kHz. The mechanic Q of the transducer is 1000. The free-mass weighs 2 grams, the transducer with the mounting platform weighs 800 grams and Earth gravity applied as the preload force.

In Fig. 13, each dot represents an impact event of the free-mass with the bit stem. The X-axis is the time that the impact happens and the Y-axis is the velocity of the free-mass before impact, normalized by the horn tip vibration velocity without loading, in this case, 6.67 m/s. The pattern looks like a random sequence of impacts. No repeat cycle has been observed. Actually, no random perturbation is added to input data of the program. The simulation is repeatable for fixed initial conditions. Therefore the simulation actually shows a pseudo-random procedure. The amplitudes of the horn vibration at the moment before horn/free-mass contact are presented in Fig. 14. The amplitudes are normalized to the horn vibration

amplitude without loading. As expected, the average amplitude is lower than that without loading because the horn loses energy while driving the free-mass.

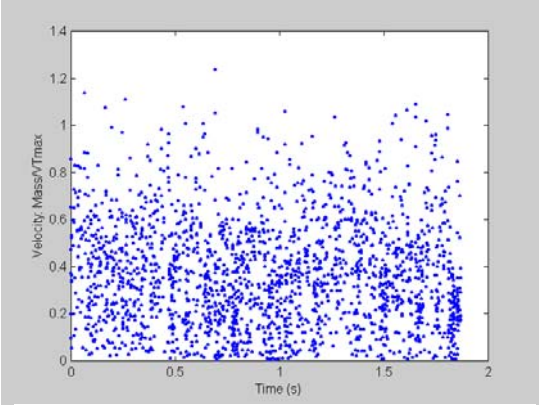

Fig. 13. Free-mass velocity normalized by the horn tip vibration velocity

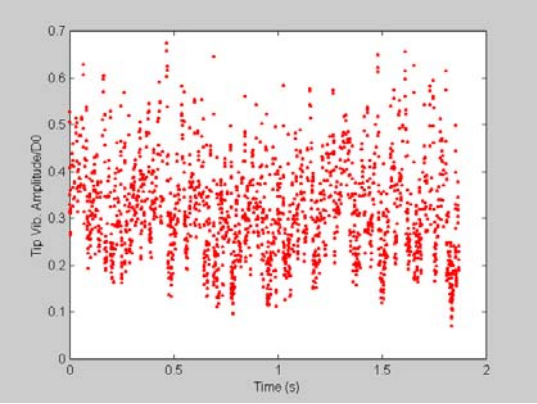

Fig. 14. Horn vibration amplitude normalized by the amplitude without loading

Fig. 15(a) shows the heights of the horn transducer in the free-mass/horn impact events. Ones can see the trace of the translation movement of the horn transducer. Fig. 15(b) shows an example of the horn movement in a drilling test. The data was obtained from images taken by a high-speed camera. The simulation results successfully showed a characteristic of the movement similar to the experimental data. The frequency, height and randomness of the jumps appear to agree very well with the data .

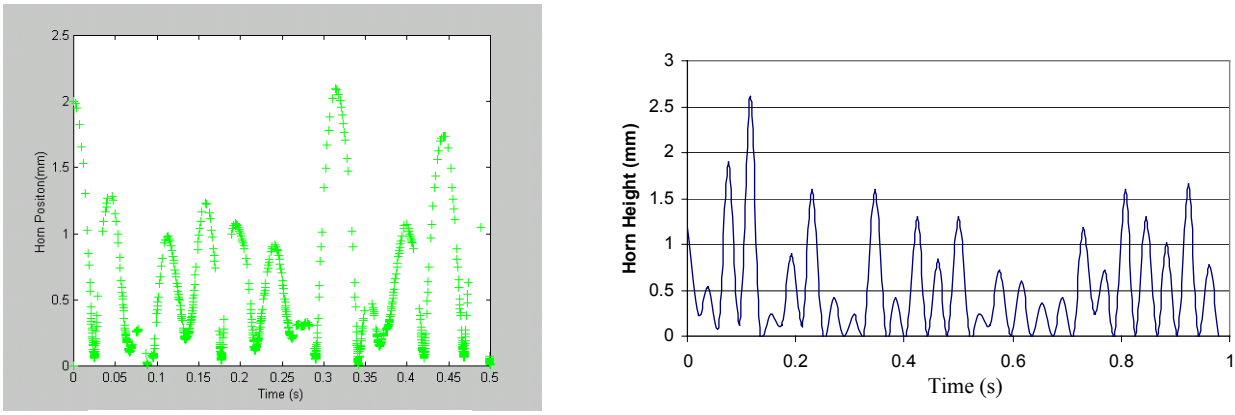

(a) A typical simulation results

(b) Typical experimental observation

Fig. 15. The body movement of the horn transducer

The average speed of the free-mass hitting the drill stem was found to be 2.4 m/s. The electric input power is 21 W and the mechanic power transferred to the drill stem is 6.5 W. The average hit frequency is 1100 Hz. The contact time of each free-mass/bit impact is short, in the range from 10 to 15 μs (see Fig. 10). Therefore, the average mechanic power delivered to the drill bit in the contact time is as high as 540 W.

The results show that, by using the free-mass to convert the high frequency vibrations to low frequency impacts, the low continuous electric input power is converted to a high mechanical power during the impact time. The later creates large enough strain in the rock to enable efficient drilling.

G. Strain and stress in rocks and estimation of drilling rate

In order to estimate the drilling rate of the impacts, a finite element model was developed using ANSYS. The model predicts the strain and stress developed in infinite half space of rock, assuming the rock has no break.

Preliminary results were derived by assuming that the rock is isotropic material with a Young's modulus of 11.2 GPa, poisons ratio of 0.3, and density of 2470 kg/m^3. The drill bit is 3 mm in diameter. The input impact loading from the drill has a peak value of 50 MPa with the same time response as shown in Fig. 11.

Contour maps of the maximum principal strain were plotted in Fig.15 and used as indication of fracture of rocks. The results show qualitative features of the rocks fracture under ultrasonic drilling. We find that the highest principal strain occurs at the edge of the drill bit. It implies that the fracture is likely going to happen at the edge, which is confirmed by viewing the high speed filming during drilling.

In order to break rock by mechanically induced stresses, sufficient force or energy must be applied to the rock in order induce stresses that exceed the rock's strength. Once this threshold value of force or energy is exceeded, the amount of energy required to break or remove a unit volume of rock remains nearly constant [8]. This energy parameter, which is a measure of the efficiency of the drill, is defined as *specific energy* [9]. The rate at which rock can be crushed, R, is defined as

$$R = P/E \qquad (21)$$

where P = power input to the rock, joules/sec;

E = specific energy, joules/cm^3.

The specific energy E and the compression strength of various types of rocks are listed in Table 2 below [9].

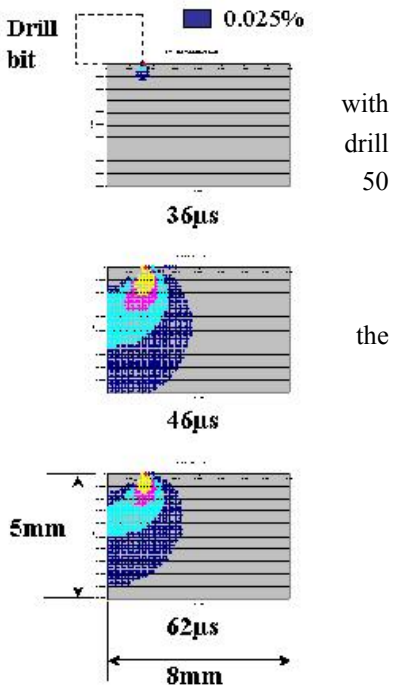

Fig. 15. The principle strain profile.

Table 2. Specific energy and compression strength of rocks

Rock type	Compression strength (MPa)	Specific energy (joules/cm^3)
Soft	< 50	30
Medium	50 – 100	50
Hard	100 – 200	260
Very hard	> 200	390

Only the part of the energy transferred from the drill bit to the rock while the stress is higher than the strength of the rock is considered as contributing to rock pulverizing. The energy is obtained from the force-displacement curve for the surface of rock under the drill bit. It should be noted that the force-displacement curve is derived under the assumption that the loading does not exceed the strength of the rock. Otherwise the curve beyond the strength will appear totally different. However, we have assumed that the energy transferred to the rock is approximately the same. The drilling rate is estimated by this energy divided by their respective specific energy.

The model was utilized to investigate and optimize the design of the USDC. The curves shown in Fig. 16 are for different combinations of maximum power and duty-cycle. The average power is maintained at 10 watts by changing the duty cycle appropriately. The experimental data of drilling rate for variety of rock sample from soft to medium-hard are marked in the figure. The data are agreed with the model prediction in general.

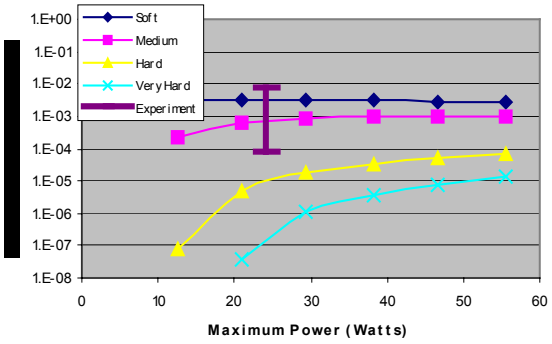

Fig. 16. Drilling rate for different maximum power (the average power is maintained at 10 watts by duty cycling the power supply). The range described by the error bar was determined experimentally from a variety of rock samples.

3. CONCLUTION

The USDC was modeled to predict its behavior towards the goal of optimizing its performance in various configurations. Physical models were developed for each section of the device and their interactions. The piezoelectric horn transducer was modeled using finite element models and with some simplifications converted to an equivalent circuit to simplify the interaction of the free-mass and electronic driver. The horn tip free-mass interaction was analyzed by a simple collision theory to explore the basic drive mechanism and by finite element approach for accuracy. A spring-mass model was developed to obtain time efficient solutions. Finite element models were also applied to the free-mass/drill bit and the drill bit/rock interactions. The program simulating the operation of the device was integrated from the models of the main parts and the interactions.

The developed models allowed for the investigation of the various interactions of the USDC. It was shown that, by using the free-mass, the continuous high frequency vibration of the horn could be converted to low frequency high mechanical power impacts. These impacts created large enough strain in the rock to enable efficient drilling. Using a simulation of the operation of the USDC the characteristics of the USDC performance were investigated and has been used to guide the design of a prototype device. The drilling rates calculated from the model were found to be in agreement with drilling rate data measured on a variety of rock samples.

REFERENCES

[1] Y. Bar-Cohen, S. Sherrit, B. Dolgin, X. Bao, Z. Chang, R. Krahe, J. Kroh, D. Pal, S. Du, T. Peterson "Ultrasonic/Sonic Driller/Corer(USDC) for planerary application," *Proc. SPIE Smart Structure and Materials 2001*, Volume 4327-55, 2001.

[2] S. Sherrit, X. Bao, Z. Chang, B. Dolgin, Y. Bar-Cohen, D. Pal, J. Kroh, T. Peterson "Modeling of the ultrasonic/sonic driller/corer: USDC," *2000 IEEE Int. Ultrason. Symp. Proc.*, 2000, vol.1,pp. 691-694.

[3] S. Sherrit, B. Dolgin, Y. Bar-Cohen, D. Pal, J. Kroh, T. Peterson, " Modeling of horns for sonic/ultrasonic applications," *1999 IEEE Int. Ultrason. Symp. Proc.*, 1999, pp. 647-651.

[4] H. Allik and T.J.R. Hughes, "Finite Element Method for Piezoelectric Vibration," *Int. J. Num. Math. Eng.*, Vol. 2, 1970, pp. 151-157.

[5] Y. Kagawa, G.M.T. Gladwell, " Finite element analysis of flexure-type vibrators with electrostrictive transducers," *IEEE Trans. Sonics Ultrason.*, vol. SU-17, 1970, pp. 41-49

[6] X. Bao, Q. Xu, D. Wang, "Vibration and acoustic radiation of piezoelectric transducers: FEM-equivalent circuit," *Sientia Sinica, Series A: Math., Phys., Astron. Tech. Scie.*, vol. 26, pp. 1285-1294, 1983.

[7] Ansys, *Elements Reference* Release 5.4, Canonsburg, PA: Ansys Inc, 1998, pp. 4-67.

[8] R. Teale, "The concept of specific energy in rock drilling," *Int. J. Rock Mech. Min. Sci*., vol. 2, pp. 57, 1965.

[9] W. Maurer, Novel Drilling Techniques, Pergamon Press, 1968.